Eur J Nucl Med Mol Imaging (2012) 39:990–1000
DOI 10.1007/s00259-012-2102-3

ORIGINAL ARTICLE

Longitudinal imaging of Alzheimer pathology using [^{11}C]PIB, [^{18}F]FDDNP and [^{18}F]FDG PET

Rik Ossenkoppele · Nelleke Tolboom · Jessica C. Foster-Dingley · Sofie F. Adriaanse · Ronald Boellaard · Maqsood Yaqub · Albert D. Windhorst · Frederik Barkhof · Adriaan A. Lammertsma · Philip Scheltens · Wiesje M. van der Flier · Bart N. M. van Berckel

Received: 2 November 2011 / Accepted: 28 February 2012 / Published online: 23 March 2012

Abstract
Purpose [^{11}C]PIB and [^{18}F]FDDNP are PET tracers for in vivo detection of the neuropathology underlying Alzheimer's disease (AD). [^{18}F]FDG is a glucose analogue and its uptake reflects metabolic activity. The purpose of this study was to examine longitudinal changes in these tracers in patients with AD or mild cognitive impairment (MCI) and in healthy controls.
Methods Longitudinal, paired, dynamic [^{11}C]PIB and [^{18}F]FDDNP (90 min each) and static [^{18}F]FDG (15 min) PET scans were obtained in 11 controls, 12 MCI patients and 8 AD patients. The mean interval between baseline and follow-up was 2.5 years (range 2.0–4.0 years). Parametric [^{11}C]PIB and [^{18}F]FDDNP images of binding potential (BP_{ND}) and [^{18}F]FDG standardized uptake value ratio (SUVr) images were generated.
Results A significant increase in global cortical [^{11}C]PIB BP_{ND} was found in MCI patients, but no changes were observed in AD patients or controls. Subsequent regional analysis revealed that this increase in [^{11}C]PIB BP_{ND} in MCI patients was most prominent in the lateral temporal lobe ($p<0.05$). For [^{18}F]FDDNP, no changes in global BP_{ND} were found. [^{18}F]FDG uptake was reduced at follow-up in the AD group only, especially in frontal, parietal and lateral temporal lobes (all $p<0.01$). Changes in global [^{11}C]PIB binding ($\rho=-0.42$, $p<0.05$) and posterior cingulate [^{18}F]FDG uptake ($\rho=0.54$, $p<0.01$) were correlated with changes in Mini-Mental-State Examination score over time across groups, whilst changes in [^{18}F]FDDNP binding ($\rho=-0.18$, $p=0.35$) were not.
Conclusion [^{11}C]PIB and [^{18}F]FDG track molecular changes in different stages of AD. We found increased amyloid load in MCI patients and progressive metabolic impairment in AD patients. [^{18}F]FDDNP seems to be less useful for examining disease progression.

Keywords Alzheimer's disease · Positron emission tomography · [^{11}C]PIB · [^{18}F]FDDNP · [^{18}F]FDG

R. Ossenkoppele (✉) · N. Tolboom · S. F. Adriaanse · P. Scheltens · W. M. van der Flier
Department of Neurology & Alzheimer Center,
VU University Medical Center,
PO Box 7057, 1007MB Amsterdam, Netherlands
e-mail: r.ossenkoppele@vumc.nl

R. Ossenkoppele · N. Tolboom · J. C. Foster-Dingley · S. F. Adriaanse · R. Boellaard · M. Yaqub · A. D. Windhorst · A. A. Lammertsma · B. N. M. van Berckel
Department of Nuclear Medicine & PET Research,
VU University Medical Center,
Amsterdam, Netherlands

W. M. van der Flier
Department of Epidemiology & Biostatistics,
VU University Medical Center,
Amsterdam, Netherlands

F. Barkhof
Department of Radiology, VU University Medical Center,
Amsterdam, Netherlands

Introduction

Alzheimer's disease (AD) is a progressive neurodegenerative disorder characterized by decline in cognitive function, progressive impairment of activities of daily living and neuropsychiatric symptoms. The neuropathological characteristics underlying AD are senile plaques consisting of

amyloid-β (Aβ) and neurofibrillary tangles consisting of hyperphosphorylated tau, possibly leading to loss of synaptic density and network connections and ultimately generalized cortical atrophy [1, 2]. Several PET tracers are currently available to assess molecular aspects of this neuropathological process in vivo. ^{18}F-2-Fluoro-2-deoxy-D-glucose ([^{18}F]FDG) is a glucose analogue and, as such, its uptake is strongly associated with neuronal function. [^{18}F]FDG is a well-validated and widely used PET tracer with a sensitivity of 94 % and a specificity of 73 % for diagnosing AD [3]. More recently, [^{11}C]PIB (Pittsburgh Compound B) [4] and [^{18}F]FDDNP (2-(1-{6-[(2-[^{18}F]fluoroethyl)(methyl)amino]-2-naphthyl}ethylidene)malononitrile) [5] have been developed for in vivo imaging of the neuropathology underlying AD.

[^{11}C]PIB has high diagnostic accuracy for the detection of AD [4, 6] and can easily be used for visual assessment [7, 8]. Furthermore, high [^{11}C]PIB binding is a strong predictor of progression of mild cognitive impairment (MCI) to AD [9–12]. Longitudinal imaging studies in AD, however, showed inconsistent results with no [13–15] or only modest [11, 16, 17] changes in [^{11}C]PIB binding over time in AD. [^{18}F]FDDNP also discriminates between AD and healthy controls on a group level [5, 6, 18], but in AD patients it has a ninefold lower specific binding signal than [^{11}C]PIB [6]. The unique feature of [^{18}F]FDDNP, however, is its affinity to bind to both amyloid plaques and neurofibrillary tangles in vitro [19]. This is important, as tangle load, rather than amyloid burden, is strongly related to both cognitive performance and disease progression. In the only published longitudinal study with [^{18}F]FDDNP to date, cognitive decline was associated with increased [^{18}F]FDDNP binding over time [5]. As such, [^{18}F]FDDNP might be a suitable, or even better, PET tracer for monitoring the time-course of the disease.

The purpose of this longitudinal study was to examine global and regional changes in specific [^{11}C]PIB and [^{18}F]FDDNP binding and [^{18}F]FDG uptake over time in the same set of patients with AD and MCI, and in healthy controls.

Methods

Subjects

At baseline, 15 subjects were included in each group [6]. In the AD group, six patients were not capable of undergoing follow-up PET scans due to disease progression, whilst one patient experienced a severe stroke. Three MCI patients refused to participate in this follow-up study due to lack of motivation. Of the MCI patients who dropped out, one progressed to AD and the others remained cognitively stable. Two healthy controls developed diseases other than dementia, one subject could not participate because of family affairs and one control was lost to follow-up. Consequently, 8 AD patients, 12 MCI patients and 11 healthy controls were included in this longitudinal study.

All subjects received a standard dementia screening at baseline that included medical history, physical and neurological examinations, screening laboratory tests, brain MRI and extensive neuropsychological testing [6]. Clinical diagnosis was established by consensus in a multidisciplinary team, without awareness of the PET results. After 2–3 years, a renewed clinical consensus diagnosis was established using repeated brain MRI, neuropsychological testing and clinical data.

All AD patients met the criteria proposed by the National Institute of Neurological and Communicative disorders and Stroke and the Alzheimer's Disease and Related Disorders Association (NINCDS-ADRDA) for probable AD [20]. At follow-up, six out of eight AD patients were taking acetylcholinesterase inhibitors and one AD patient was taking a selective serotonin reuptake inhibitor. MCI patients of the amnestic subtype met the Petersen criteria based on subjective and objective cognitive impairment, in the absence of dementia or significant functional loss [21]. At follow-up, one MCI patient was taking an acetylcholinesterase inhibitor and another a benzodiazepine. Controls were recruited through advertisements in newspapers and underwent the same diagnostic procedures. None of the controls was taking psychotropic medication on either occasion or developed cognitive complaints.

Exclusion criteria were a history of major psychiatric or neurological illness (other than AD) and the use of nonsteroidal antiinflammatory drugs, as the latter have been reported to compete with [^{18}F]FDDNP for binding to Aβ fibrils in vitro and to Aβ plaques ex vivo [19]. Additional exclusion criteria for controls were subjective memory complaints or clinically relevant abnormalities on MRI. Patients with severe vascular events during the follow-up period, such as stroke or haemorrhage, were also excluded. Written informed consent was obtained from all subjects after a complete written and verbal description of the study. The study protocol was approved by the Medical Ethics Review Committee of the VU University Medical Center.

PET

[^{11}C]PIB and [^{18}F]FDDNP PET scans were performed on the same day, except in five subjects at baseline (one AD, three MCI, one control) and in seven subjects at follow-up (three AD, three MCI, one control), all due to radiosynthesis failure. PET scans were obtained on an ECAT EXACT HR+ scanner (Siemens/CTI; Knoxville, TN) equipped with a neuroinsert to reduce the contribution of scattered photons. This scanner enables the acquisition of 63 transaxial planes

over a 15.5-cm axial field of view, thus allowing the whole brain to be imaged in one bed position. The properties of this scanner have been reported elsewhere [22]. All subjects received a venous cannula for tracer injection. First, a 10-min transmission scan was obtained in two-dimensional acquisition mode using three retractable rotating line sources. This scan was used to correct the subsequent emission scan for photon attenuation. Next, a dynamic emission scan in three-dimensional acquisition mode was started simultaneously with the intravenous injection of [^{11}C]PIB (351±82 MBq at baseline and 377±91 MBq at follow-up) using an infusion pump (Med-Rad, Beek, The Netherlands) at a rate of 0.8 ml s^{-1}, followed by a flush of 42 ml saline at 2.0 ml s^{-1}. [^{11}C]PIB was synthesized according to the procedure of Wilson et al. with modification [23], resulting in a specific activity of 41±22 GBq μmol^{-1} (at baseline) and 88±40 GBq μmol^{-1} (at follow-up). The [^{11}C]PIB scan consisted of 23 frames increasing progressively in duration (1×15, 3×5, 3×10, 2×30, 3×60, 2×150, 2×300, 7×600 s) for a total scan duration of 90 min. Finally, after a rest period of at least an hour to allow decay of ^{11}C, exactly the same procedure was repeated but now using an injection of [^{18}F]FDDNP [24] (177±14 MBq at baseline and 189±15 MBq at follow-up) with a specific activity of 86±51 GBq μmol^{-1} (at baseline) and 70±43 GBq μmol^{-1} (at follow-up). Patient motion was restricted by a head holder and regularly checked during scanning using laser beams.

[^{18}F]FDG PET scans were obtained in all subjects within an average of 1 month of the [^{11}C]PIB and [^{18}F]FDDNP scans. [^{18}F]FDG was injected after subjects had rested for 10 min with their eyes closed and ears unplugged in a dimly lit room with minimal background noise. A bolus of FDG (150±17 MBq at baseline and 186±7 MBq at follow-up) was injected intravenously, and 35 min later, a 10-min transmission scan followed by a 15-min emission scan (3 × 5-min frames) were performed.

MRI

All subjects underwent repeated structural MRI scans using a 1.5 T Sonata scanner (Siemens, Erlingen, Germany). The scan protocol included a coronal T1-weighted three-dimensional magnetization prepared rapid acquisition gradient echo (MPRAGE) sequence (slice thickness 1.5 mm, 160 slices, matrix size 256×256, voxel size 1×1×1.5 mm, echo time 3.97 ms, repetition time 2,700 ms, inversion time 950 ms, flip angle 8°) and was used for coregistration, segmentation and definition of regions of interest (ROI).

Image and data analysis

All PET sinograms were corrected for dead time, tissue attenuation using the transmission scan, decay, scatter and randoms. Next, data were reconstructed using a standard filtered back-projection algorithm and a Hanning filter with a cut-off at 0.5 times the Nyquist frequency. A zoom factor of 2 and a matrix size of 256 × 256 × 63 were used, resulting in a voxel size of 1.2×1.2×2.4 mm and spatial resolution of approximately 7 mm full-width at half-maximum at the centre of the field of view.

MR images were aligned with corresponding PET images using a mutual information algorithm. Data were further analysed using PVE-lab, a software program that uses a probability map based on 35 delineated ROIs that have been validated previously [25]. ROIs were projected onto [^{11}C]PIB and [^{18}F]FDDNP parametric nondisplaceable binding potential (BP_{ND}) images. These parametric images were generated using a two-step basis function implementation of the simplified reference tissue model (RPM2) [26], together with the full dynamic 90-min PET data. RPM2, a fully quantitative method for assessing the data, was identified as the parametric model of choice [26–28]. BP_{ND} is a quantitative measure of specific binding and reflects the concentration of specifically bound tracer relative to that of free plus nonspecifically bound tracer in tissue at equilibrium. For [^{18}F]FDG, standardized uptake value ratio (SUVr) images (45–60 min after injection) were generated. The cerebellar grey matter was chosen as the reference tissue for this triplet of PET tracers because of its (histopathological) lack of plaques positive for Congo red and thioflavin-S, and its insensitivity to metabolic changes during disease progression [29].

For regional analysis, BP_{ND} ([^{11}C]PIB and [^{18}F]FDDNP) and SUVr ([^{18}F]FDG) of the frontal (volume-weighted average of orbital frontal, medial inferior frontal and superior frontal), parietal and lateral temporal (volume-weighted average of superior temporal and medial inferior temporal) cortices, and the medial temporal lobe (MTL; volume-weighted average of the entorhinal cortex and the hippocampus) and posterior cingulate were calculated. In addition, two global cortical ROIs were defined. First, for direct comparison between [^{11}C]PIB and [^{18}F]FDDNP, a global cortical BP_{ND} based on the volume-weighted average of the frontal, parietal and lateral temporal cortices, MTL, and posterior cingulate was computed. Second, another global cortical BP_{ND} excluding the MTL was calculated as this brain region shows substantially less amyloid deposition than the other regions [4, 6]. Finally, [^{11}C]PIB scans were classified as either positive or negative, based on visual inspection of parametric BP_{ND} images by a trained nuclear medicine physician (B.v.B.).

Statistics

Group differences in subject characteristics were assessed using one-way analysis of variance (ANOVA) with post

hoc least significant difference (LSD) tests. Longitudinal changes in global cortical BP_{ND} and SUVr were assessed using ANOVA for repeated measures with diagnosis as the between subjects factor, time as the within subjects factor and global cortical BP_{ND} and SUVr as variables. Next, groups were stratified according to baseline global [^{11}C]PIB BP_{ND} (<0.1, 0.1–0.75 and >0.75) and paired-sample *t*-tests were performed between baseline and follow-up global measures of [^{11}C]PIB, [^{18}F]FDDNP and [^{18}F]FDG. Subsequently, regional changes over time were investigated using paired-sample *t*-tests in each group separately. Spearman correlation analysis was used to assess the relationships between changes in global cortical BP_{ND} and SUVr and changes in Mini-Mental-State Examination (MMSE) scores over time and the relationships between changes in global cortical [^{11}C]PIB BP_{ND} and [^{18}F]FDDNP BP_{ND} and posterior cingulate [^{18}F]FDG SUVr. The level of significance was set at $p<0.05$, except for the interaction terms in ANOVA for repeated measures, where $p<0.10$ was considered significant.

Results

The three subject groups did not differ with respect to age, gender, education or mean interval between baseline and follow-up (Table 1). MMSE scores decreased over time in MCI and AD patients ($p<0.05$) and remained stable in controls. During the follow-up period, four MCI patients progressed to AD and one converted to frontotemporal lobar degeneration. Two MCI patients demonstrated clear cognitive improvement and were no longer classified as MCI at follow-up. The other five MCI patients remained cognitively stable.

[^{11}C]PIB

At baseline, global cortical BP_{ND} for [^{11}C]PIB was 0.87±0.10 in AD patients, 0.39±0.39 in MCI patients and 0.12±0.27 in controls. At follow-up, global cortical BP_{ND} was 0.86±0.13 in AD patients, 0.46±0.39 in MCI patients and

Table 1 Demographic and clinical characteristics according to subject group. The data are presented as means±SD unless otherwise indicated

Variable	Controls (n=11)	MCI (n=12)	AD (n=8)	P value
Age at baseline (years)	66±7	67±7	62±6	0.23
Sex				
Percent male	73	75	87	0.60
Male/female (n)	8/3	9/3	7/1	
Apolipoprotein ε4				
0	9	4	2	<0.05
1	2	5	4	
2	0	3	2	
Education[a], median (range)	6 (2–7)	6 (3–7)	6 (4–7)	0.58
Baseline to follow-up interval (years)	2.5±0.3	2.5±0.5	2.7±0.6	0.49
MMSE, baseline	29±1	27±3	25±2	<0.0001[b]
MMSE, follow-up	29±1	25±1**	22±5**	<0.0001[c]
RAVLT, baseline				
Immediate recall	37±10	29±5	27±5	<0.05[d]
Delayed recall	7±2	3±3	2±2	<0.05[d]
Recognition	29±5	27±2	24±3	<0.05[e]
RAVLT, follow-up				
Immediate recall	39±13	29±10	20±4	<0.05[d]
Delayed recall	8±4	3±4	1±1	<0.05[d]
Recognition	28±4	26±3	22±5	<0.05[e]

RAVLT Rey auditory verbal learning test.

Differences between groups (*P* values) were assessed using one-way ANOVA (age at baseline, mean interval, MMSE and RAVLT), Kruskal-Wallis test(sex, apolipoprotein ε4 status and education) and paired-sample *t*-test (changes over time in MMSE and RAVLT scores).

**$p<0.05$, decline in MMSE during follow-up.

[a] Using Verhage's classification [41] on a scale of 1–7.

[b] Post-hoc LSD tests: AD < MCI, $p<0.05$; AD < controls, $p<0.0001$; MCI < controls, $p<0.05$.

[c] Post-hoc LSD tests: AD < MCI, $p<0.05$; AD < controls, $p<0.0001$; MCI < controls, $p<0.01$.

[d] Post-hoc LSD tests: AD < HC, $p<0.05$, MCI < HC, $p<0.05$.

[e] Post-hoc LSD tests: AD < MCI, $p<0.05$, AD < HC, $p<0.05$.

0.15±0.29 in controls. Figure 1 (top row) shows the changes over time for each individual subject in the three groups. Four out of five PIB-positive amnestic MCI patients progressed to AD during the follow-up period. The two MCI subjects with the lowest BP_{ND} at baseline showed clear cognitive improvement and were no longer classified as MCI patients at follow-up. Furthermore, one PIB-negative MCI patient converted to frontotemporal lobe degeneration, and the other PIB-negative MCI patients remained cognitively stable. ANOVA for repeated measures showed a main effect for diagnosis ($p<0.05$), but no significant main effect for time ($p=0.08$). There was no significant interaction between time and diagnosis for global cortical BP_{ND} including the MTL ($p=0.11$). There was an interaction, however, between time and diagnosis for global cortical BP_{ND} excluding the MTL ($p<0.10$), which was attributable to an increase in [^{11}C]PIB binding over time in the MCI group (Fig. 1). Subsequent regional analysis using paired-sample *t*-tests in the subject groups revealed a significant increase in [^{11}C]PIB binding in the lateral temporal lobe in the MCI group ($p<0.05$, Table 2). [^{11}C]PIB binding in the MTL in the AD group decreased over time ($p<0.05$). Correlation analysis using Spearman's ρ revealed a negative correlation between increase in global cortical [^{11}C]PIB binding and decline in MMSE scores across the groups ($\rho=-0.42$, $p<0.05$, Fig. 2a). There was a modest, albeit nonsignificant, correlation between changes in global [^{11}C]PIB and [^{18}F]FDDNP BP_{ND} across groups ($\rho=0.33$, $p=0.08$). Changes in global [^{11}C]PIB BP_{ND}, however, did not correlate with change in global [^{18}F]FDG SUVr ($\rho=0.02$, $p=0.94$). In paired sample *t*-tests, subjects with low amyloid burden at baseline ([^{11}C]PIB BP_{ND} <0.1) showed no significant changes in [^{11}C]PIB binding ($p=0.09$), [^{18}F]FDDNP binding ($p=0.72$) or [^{18}F]FDG uptake ($p=0.99$) over time

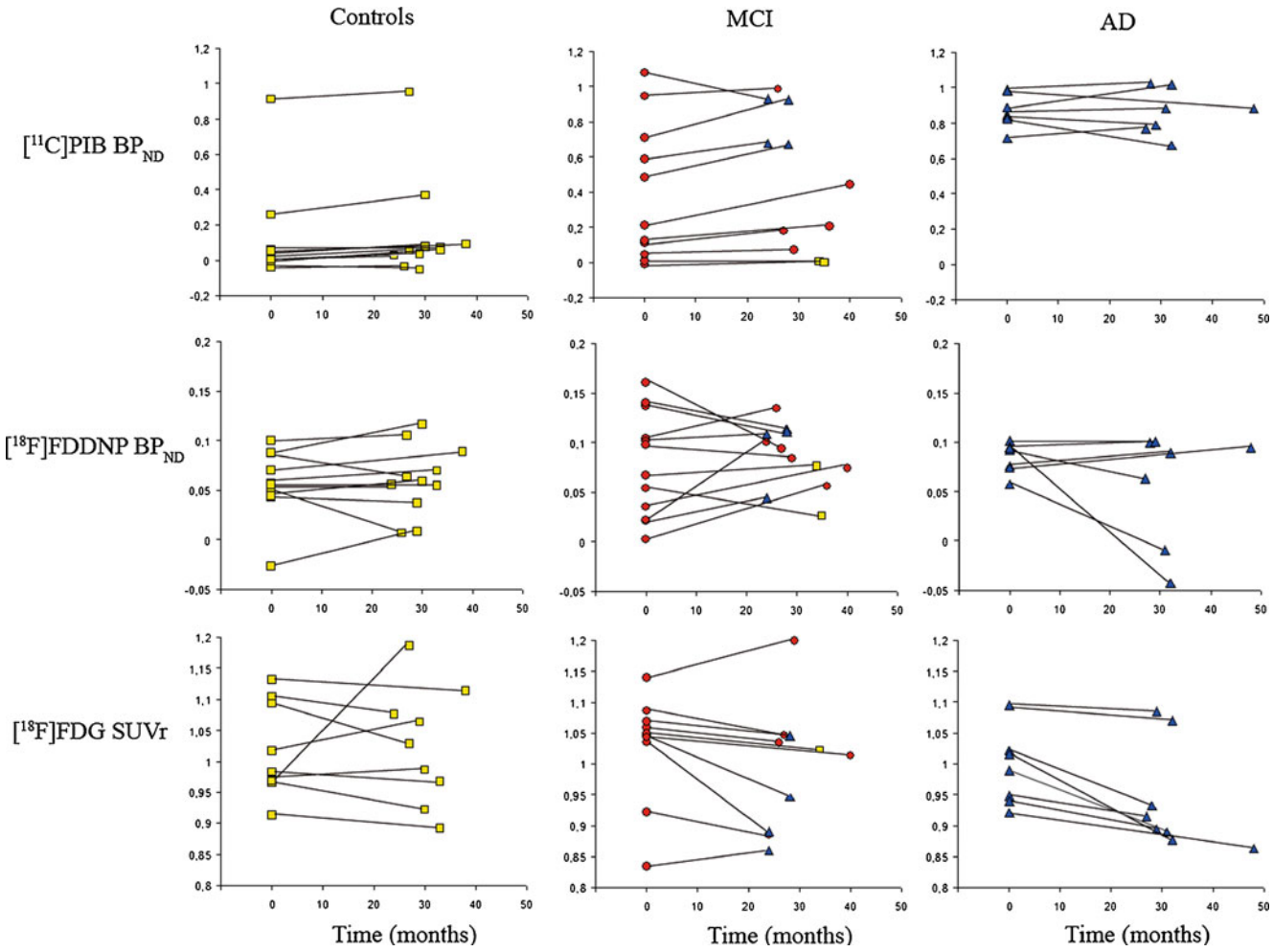

Fig. 1 Overview of global cortical [^{11}C]PIB BP_{ND} (*top row*), [^{18}F]FDDNP BP_{ND} (*middle row*) and [^{18}F]FDG SUVr (*bottom row*) in the same healthy controls (*left*), MCI patients (*centre*) and AD patients (*right*). In the MCI group, several diagnoses changed during the follow-up period. The *X*-axis represents the follow-up period in months. Baseline and follow-up measurements are connected for each individual subject. ANOVA for repeated measures revealed increased [^{11}C]PIB binding in the MCI group and decreased [^{18}F]FDG uptake in the AD group over time. No longitudinal changes in [^{18}F]FDDNP binding were found

Table 2 Regional [^{11}C]PIB BP_{ND} over time by subject group

Region	Controls		MCI		AD	
	Baseline	Follow-up	Baseline	Follow-up	Baseline	Follow-up
Frontal	0.13±0.33	0.15±0.34	0.43±0.44	0.50±0.43	0.93±0.09	0.94±0.14
Parietal	0.12±0.27	0.15±0.28	0.39±0.42	0.47±0.39	0.95±0.20	0.93±0.19
Posterior cingulate	0.12±0.21	0.14±0.23	0.41±0.43	0.44±0.40	0.88±0.18	0.82±0.21
MTL	0.09±0.09	0.06±0.08	0.09±0.07	0.08±0.07	0.18±0.04	0.12±0.06**
Temporal	0.12±0.24	0.14±0.26	0.38±0.36	0.46±0.39*	0.81±0.10	0.79±0.12

*$p<0.05$, increased binding; **$p<0.05$, decreased binding; paired-sample *t*-tests.

(Tables 3 and 4). Subjects with a baseline [^{11}C]PIB BP_{ND} between 0.1 and 0.75 showed increased [^{11}C]PIB binding ($p<0.01$) and decreased [^{18}F]FDG uptake ($p<0.05$) during the follow-up period, whilst [^{18}F]FDDNP binding did not change ($p=0.95$). Subjects with high amyloid burden at baseline ([^{11}C]PIB BP_{ND} >0.75) showed a marked decrease in [^{18}F]FDG uptake ($p<0.01$) over time, whereas [^{11}C]PIB binding ($p=0.63$) and [^{18}F]FDDNP binding ($p=0.71$) remained stable.

[^{18}F]FDDNP

At baseline, global cortical BP_{ND} for [^{18}F]FDDNP was 0.08±0.02 in AD patients, 0.08±0.05 in MCI patients and 0.06±0.04 in controls. At follow-up, global cortical BP_{ND} was 0.06±0.06 in AD patients, 0.09±0.03 in MCI patients and 0.06±0.04 in controls. Figure 1 (middle row) shows individual changes over time for the three groups. The majority of AD patients and two of the four MCI converters showed a nonsignificant decrease in [^{18}F]FDDNP binding over time. ANOVA for repeated measures showed no main effect of diagnosis ($p=0.28$) or time ($p=0.45$), nor was there an interaction between diagnosis and time ($p=0.16$). These results did not change when the MTL was left out of the global ROI. Subsequent regional analysis within groups showed an increase in specific [^{18}F]FDDNP binding in the parietal lobe ($p<0.05$) and a decrease in the MTL ($p<0.05$) in the healthy controls. All other brain areas in the subject groups remained unchanged (Table 4). There was no correlation between changes in global [^{18}F]FDDNP binding and MMSE scores over time ($\rho=-0.18$, $p=0.35$, Fig. 2b). Changes in global [^{18}F]FDDNP BP_{ND} did not correlate with changes in global [^{18}F]FDG SUVr ($\rho=0.14$, $p=0.51$).

Table 3 Longitudinal changes in global [^{11}C]PIB binding, [^{18}F]FDDNP binding and [^{18}F]FDG uptake in relation to baseline global [^{11}C]PIB BP_{ND}

	Baseline [^{11}C]PIB BP_{ND}		
	<0.1 ($n=12$)	0.1–0.75 ($n=9$)	>0.75 ($n=9$)
Change in [^{11}C]PIB BP_{ND}	0.01±0.03	0.13±0.07**	−0.02±0.11
Change in [^{18}F]FDDNP BP_{ND}	0.00±0.08	−0.00±0.04	−0.01±0.06
Change in [^{18}F]FDG SUVr	0.00±0.08	−0.03±0.03*	−0.08±0.07**

*$p<0.05$, **$p<0.01$, paired-sample *t*-tests.

[^{18}F]FDG

Global cortical SUVr for [^{18}F]FDG at baseline was 1.00±0.07 in AD, 1.03±0.09 in MCI patients and 1.02±0.08 in controls. At follow-up, global cortical SUVr was 0.93±0.07 in AD patients, 1.00±0.10 in MCI patients and 1.03±0.09 in controls. Figure 1 (*bottom row*) shows individual changes over time in all subjects in the three groups. A progressive decrease in [^{18}F]FDG uptake was observed in all AD patients and in three of four MCI converters. ANOVA for repeated measures showed no main effect of diagnosis ($p=0.30$), but there was a main effect of time ($p<0.05$), and there was an interaction between time and diagnosis ($p<0.05$). The observed decrease in [^{18}F]FDG uptake over time was largely attributable to patients with AD (Fig. 1). Subsequent regional analysis in the AD patients showed decreased glucose metabolism in the frontal ($p<0.01$), parietal ($p<0.01$) and lateral temporal lobes ($p<0.01$) over time, but not in the posterior cingulate ($p=0.09$) or MTL ($p=0.42$). No regional changes over time were observed in the controls or MCI patients (Table 5). Changes in [^{18}F]FDG uptake in the posterior cingulate gyrus were correlated with the decline in MMSE scores across the groups ($\rho=0.54$, $p<0.01$, Fig. 2c).

Discussion

In this study, temporal changes in specific [^{11}C]PIB and [^{18}F]FDDNP binding and in [^{18}F]FDG uptake were investigated using repeat scans in the same set of AD patients, MCI patients and control subjects. We found an increase in [^{11}C]PIB in the MCI patients which was most prominent in the lateral temporal lobe. No changes in the AD patients and the controls were observed. [^{18}F]FDDNP binding did not change

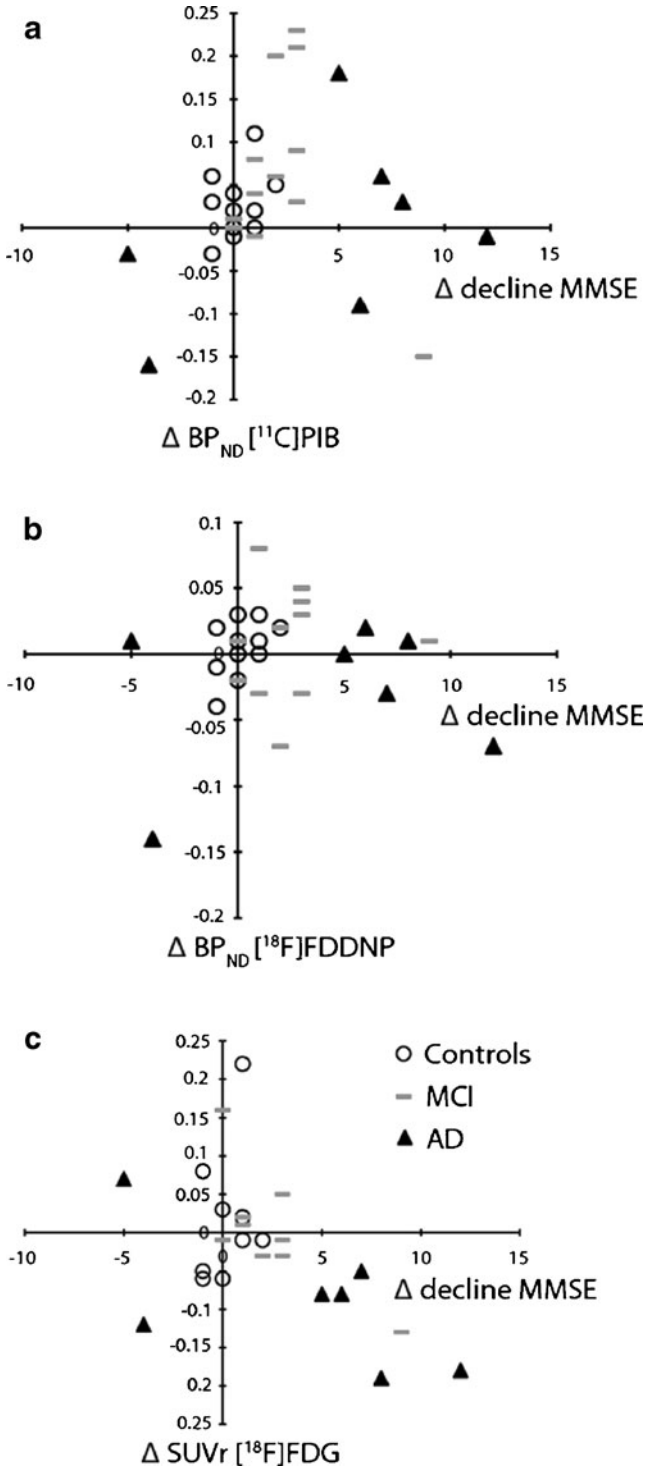

Fig. 2 Correlation analysis (Spearman's ρ) of the relationships between changes in global cortical BP_{ND} and posterior cingulate SUVr and decline in MMSE scores over time. Across the groups, there were moderate correlations between [^{11}C]PIB BP_{ND} ($\rho=-0.42$, $p<0.05$) and [^{18}F]FDG SUVr ($\rho=0.54$, $p<0.01$) and MMSE. No significant correlation was found between [^{18}F]FDDNP BP_{ND} and MMSE ($\rho=-0.18$, $p=0.35$). (*filled triangles* AD patients, *circles* MCI patients, *squares* controls)

over time in any of the groups. [^{18}F]FDG uptake decreased over time in the AD patients only, particularly in the frontal, parietal and lateral temporal cortices. Changes in global [^{11}C]PIB binding and [^{18}F]FDG uptake in the posterior cingulate were correlated with changes in MMSE scores over time across subject groups, whilst changes in [^{18}F]FDDNP were not.

Recently, Jack et al. [30] proposed a biomarker model based on the assumption that the formation of senile plaques reaches a relative plateau by the time clinical symptoms emerge. The present data, however, show increased [^{11}C]PIB binding over time in the vast majority of both MCI converters and nonconverters. This finding is in agreement with three recent studies in which longitudinal changes in amyloid load in MCI patients were also identified using [^{11}C]PIB [11, 12, 16]. The dynamic change in [^{11}C]PIB binding over time during the MCI stage is exemplified by a cognitively stable MCI patient in whom the baseline PIB scan was negative and the follow-up scan was positive (Fig. 3). This particular finding is not consistent with the aforementioned neuropathological pathway in AD patients, and suggests that cognitive complaints at the time of initial MCI diagnosis may have been driven by other pathological processes than fibrillary Aβ in this patient. Four out of five PIB-positive MCI patients progressed to AD during the follow-up period, whilst this did not happen to any of the PIB-negative MCI patients. Interestingly, the two MCI subjects with the lowest [^{11}C]PIB binding at baseline showed clear cognitive improvement and were no longer classified as MCI at follow-up. These findings together with previous reports [9–12] show that a [^{11}C]PIB-positive scan strongly predicts progression to AD in MCI patients and underscore the high negative predictive value of [^{11}C]PIB in AD.

Despite progression of disease, as indicated by a decline in MMSE score, [^{11}C]PIB BP_{ND} in AD patients was stable over time. This finding is in agreement with the amyloid cascade hypothesis [31] which states that accumulation of Aβ during early stages of the disease precedes a cascade of neuropathological events that eventually leads to AD. In later stages of the disease, the equilibrium between amyloid deposition and resolution is restored, leading to stable amyloid levels. The observed amyloid plateau in the present AD patients is consistent with data from post-mortem studies [32] and transgenic mouse models [33], as well as cerebrospinal fluid studies [34]. Furthermore, these results are in accordance with some [13–15] but not all [11, 16, 17] previous longitudinal studies using [^{11}C]PIB in AD.

In a previous study [7], it was shown that the diagnostic accuracy of [^{18}F]FDDNP for the detection of AD is lower than that of [^{11}C]PIB. Both tracers bind to fibrillar aggregates of senile plaques, although [^{3}H]FDDNP has a tenfold lower affinity than [^{3}H]PIB in vitro (8.5±1.3 nM versus 85.0±2.0 nM) [35]. This is reflected by a lower signal-to-noise ratio in vivo with a ninefold lower BP_{ND} (0.09±0.02

Table 4 Regional [^{18}F]FDDNP BP_{ND} over time by subject group

Region	Controls		MCI		AD	
	Baseline	Follow-up	Baseline	Follow-up	Baseline	Follow-up
Frontal	0.05±0.04	0.06±0.05	0.08±0.06	0.08±0.04	0.08±0.02	0.06±0.07
Parietal	0.02±0.05	0.05±0.04*	0.04±0.04	0.05±0.02	0.04±0.02	0.02±0.06
Posterior cingulate	0.06±0.03	0.03±0.04	0.06±0.07	0.06±0.04	0.08±0.05	0.04±0.07
MTL	0.12±0.04	0.11±0.03**	0.12±0.05	0.13±0.04	0.15±0.05	0.10±0.03
Temporal	0.08±0.03	0.07±0.04	0.09±0.06	0.11±0.04	0.10±0.02	0.07±0.06

*$p<0.05$, increased binding; **$p<0.05$, decreased binding; paired-sample t-tests.

versus 0.85±0.10) in AD patients [6]. It should be noted, however, that uptake of [^{18}F]FDDNP in vitro results from binding to both amyloid plaques and neurofibrillary tangles [19]. Furthermore, [^{18}F]FDDNP BP_{ND} showed strong correlations with tau levels in cerebrospinal fluid [36] and performance in episodic memory tasks [37]. It was therefore hypothesized that [^{18}F]FDDNP might be an eligible PET tracer for monitoring the time-course of the disease. This hypothesis could not be confirmed as no longitudinal changes in [^{18}F]FDDNP binding and no relationship between disease progression and increases in global [^{18}F]FDDNP BP_{ND} were observed. We were thus unable to replicate the only longitudinal study on [^{18}F]FDDNP published to date in which cognitive decline was associated with increased [^{18}F]FDDNP binding over time [5]. This can possibly be explained by several methodological considerations such as differences in subject selection and the use of different kinetic models for the analysis of PET data. More importantly, however, in the aforementioned study, repeat [^{18}F]FDDNP PET scans were only performed in a subset (nine controls and three MCI subjects) of the baseline participants (83 subjects in total). In contrast, in the present study repeat measurements were performed not only in controls and MCI patients, but also in AD patients. This larger study population allowed a statistical analysis of the longitudinal data, rather than only exploring a subset of the study sample.

However, all of the above does not explain why no increase in [^{18}F]FDDNP binding over time was found in either AD patients or MCI converters, as it is known that tangle pathology is closely related to disease progression. Therefore, the stable [^{18}F]FDDNP levels over time may be modified by reduced availability of binding sites due to brain atrophy, in particular because [^{18}F]FDDNP binding is highest in the MTL. Another consideration is that the component of [^{18}F]FDDNP that binds to neurofibrillary tangles may not be as substantial [35] as initially suggested [19]. The low BP_{ND} of [^{18}F]FDDNP further complicates its interpretation and applicability.

Progressive decrease in glucose metabolism throughout the neocortex was observed in the AD patients only. The utility of [^{18}F]FDG PET for monitoring disease progression has been found consistently in previous studies [14, 38]. The absence of a correlation between temporal changes in global [^{18}F]FDG SUVr and [^{11}C]PIB BP_{ND} across groups, together with interaction effects in different diagnostic groups indicate that both tracers track molecular changes in different stages of AD. In early stages of the disease, accumulation of Aβ is an ongoing event while no or only minor metabolic changes occur. As the clinical course of AD progresses, the amyloid curve flattens and evident generalized glucose hypometabolism arises. This notion is supported by a previous study showing that metabolic impairment follows anatomical patterns of amyloid deposition with a temporal delay [39]. For diagnostic purposes, [^{18}F]FDG and [^{11}C]PIB PET provide complementary information and can be used in combination for early and accurate detection of AD. The time-course of AD should preferably be monitored by [^{18}F]FDG.

Table 5 Regional [^{18}F]FDG SUVr over time by subject group

Region	Controls		MCI		AD	
	Baseline	Follow-up	Baseline	Follow-up	Baseline	Follow-up
Frontal	1.07±0.09	1.08±0.12	1.05±0.22	1.05±0.10	1.10±0.07	1.03±0.07*
Parietal	1.07±0.08	1.10±0.10	1.10±0.06	1.06±0.19	0.95±0.14	0.86±0.17*
Posterior cingulate	1.09±0.09	1.11±0.11	1.10±0.07	1.10±0.11	0.98±0.17	0.91±0.19
MTL	0.75±0.03	0.74±0.04	0.79±0.20	0.73±0.08	0.75±0.05	0.73±0.10
Temporal	1.00±0.07	1.00±0.09	1.04±0.09	0.97±0.10	0.97±0.07	0.88±0.09*

*$p<0.01$, decreased uptake; paired-sample t-tests.

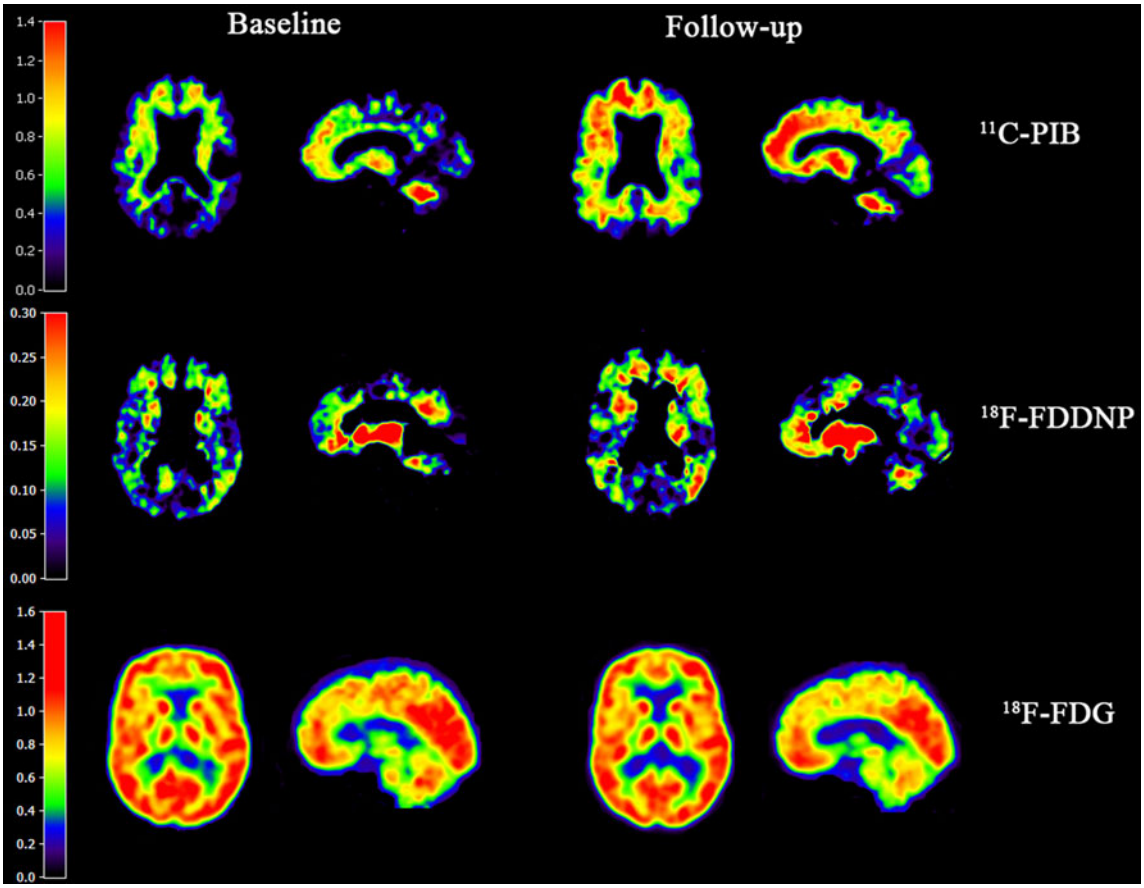

Fig. 3 Baseline and follow-up parametric [^{11}C]PIB BP_{ND} (*top row*) and [^{18}F]FDDNP BP_{ND} (middle row) and [^{18}F]FDG SUVr (*bottom row*) images in a patient with MCI, who did not convert to AD during the follow-up period. The [^{11}C]PIB PET scans show a clear shift from predominantly nonspecific binding in subcortical structures at baseline towards generalized cortical binding at follow-up. The latter pattern is typically observed in patients with AD. In addition, the [^{18}F]FDDNP scans display increased cortical binding over time. The [^{18}F]FDG scans show minor longitudinal changes, but both baseline and follow-up scans are within the normal range. A longer follow-up would be needed to determine whether the increased amyloid burden eventually leads to progression to AD

One of the strengths of the present study was its unique design that allowed direct comparison of repeat [^{11}C]PIB, [^{18}F]FDDNP and [^{18}F]FDG PET scans in the same set of patients with AD and MCI and in controls. For both [^{11}C]PIB and [^{18}F]FDDNP, optimal quantitative parametric methods were used. RPM2 provided an estimate of specific binding that is independent of potential blood flow changes, which can occur during disease progression. In contrast, semiquantitative methods such as SUVr are more sensitive to alterations in blood flow and/or tracer delivery. On the other hand, RPM2 required a dynamic PET scan of 90 min, which may have led to diminished participation in the AD group. This could have introduced some selection bias, since patients with major disease progression were not able to participate in the follow-up condition. This, in turn, is reflected by the relatively small decline in MMSE scores (Table 1) in AD patients. Furthermore, sample sizes of the subject groups were relatively small, thereby diminishing the statistical power. Another possible limitation of this study is that subjects were relatively young, and the time-course of the disease may differ between younger and older AD patients [40]. Finally, the use of acetylcholinesterase inhibitors by several AD patients may have affected the semiquantitative assessment of [^{18}F]FDG uptake.

In summary, increased cortical [^{11}C]PIB binding was seen in MCI patients and decreased [^{18}F]FDG uptake in AD patients. Based on the limited series of patients in the present study, [^{18}F]FDDNP seems to be of less value for monitoring disease progression.

Acknowledgments This work was financially supported by the Internationale Stichting Alzheimer Onderzoek (ISAO, grant 05512) and the American Health Assistance Foundation (AHAF, grant A2005-026).

Conflicts of interest None.

References

1. Cummings JL. Alzheimer's disease. N Engl J Med. 2004;351:56–67.
2. Stam CJ, de Haan W, Daffertshofer A, Jones BF, Manshanden I, van Cappellen van Walsum AM, et al. Graph theoretical analysis of magnetoencephalographic functional connectivity in Alzheimer's disease. Brain. 2009;132:213–24.
3. Silverman DHS, Small GW, Chang CY, Lu CS, de Aburto MAK, Chen W, et al. Positron emission tomography in evaluation of dementia. JAMA. 2001;286:2120–7.
4. Klunk WE, Engler H, Nordberg A, Wang Y, Blomquist G, Holt DP, et al. Imaging brain amyloid in Alzheimer's disease with Pittsburgh Compound-B. Ann Neurol. 2004;55:306–19.
5. Small GW, Kepe V, Ercoli LM, Siddarth P, Bookheimer SY, Miller KJ, et al. PET of brain amyloid and Tau in mild cognitive impairment. N Engl J Med. 2006;355:2652–63.
6. Tolboom N, Yaqub M, van der Flier WM, Boellaard R, Luurtsema G, Windhorst AD, et al. Detection of Alzheimer pathology in vivo using both 11C-PIB and 18F-FDDNP PET. J Nucl Med. 2009;50:191–7.
7. Tolboom N, Flier WM, Boverhoff J, Yaqub M, Wattjes M, Raijmakers PG, et al. Molecular imaging in the diagnosis of Alzheimer's disease: visual interpretation of [11C]PIB and [18F]FDDNP PET images. J Neurol Neurosurg Psychiatry. 2010;81:882–4.
8. Ng S, Villemagne VL, Berlangieri S, Lee ST, Cherk M, Gong SJ, et al. Visual assessment versus quantitative assessment of 11C-PIB PET and 18F-FDG PET for detection of Alzheimer's disease. J Nucl Med. 2007;48:547–52.
9. Forsberg A, Engler H, Almkvist O, Blomquist G, Hagman G, Wall A, et al. PET imaging of amyloid deposition in patients with mild cognitive impairment. Neurobiol Aging. 2008;29:1456–65.
10. Okello A, Koivunen J, Edison P, Archer HA, Turkheimer FE, Nagren K, et al. Conversion of amyloid positive and negative MCI to AD over 3 years: an 11C-PIB PET study. Neurology. 2009;73:754–60.
11. Villemagne VL, Pike K, Chetelat G, Ellis KA, Mulligan R, Bourgeat P, et al. Longitudinal assessment of Aβ and cognition in aging and Alzheimer disease. Ann Neurol. 2011;69:181–92.
12. Koivunen J, Scheinin M, Virta JR, Aalto S, Vahlberg T, Nagren K, et al. Amyloid PET imaging in patients with mild cognitive impairment: a 2-year follow-up study. Neurology. 2011;76:1085–90.
13. Engler H, Forsberg A, Almkvist O, Blomquist G, Larsson E, Savitcheva I, et al. Two-year follow-up of amyloid deposition in patients with Alzheimer's disease. Brain. 2006;129:2856–66.
14. Kadir A, Almkvist O, Forsberg A, Wall A, Engler H, Långström B, et al. Dynamic changes in PET amyloid and FDG imaging at different stages of Alzheimer's disease. Neurobiol Aging 2012;33:198.e1–14.
15. Scheinin NM, Aalto S, Koikkalainen J, Lotjonen J, Karrasch M, Kemppainen N, et al. Follow-up of [11C]PIB uptake and brain volume in patients with Alzheimer disease and controls. Neurology. 2009;73:1186–92.
16. Jack Jr CR, Lowe VJ, Weigand SD, Wiste HJ, Senjem ML, Knopman DS, et al. The Alzheimer's disease neuroimaging initiative. Serial PIB and MRI in normal, mild cognitive impairment and Alzheimer's disease: implications for sequence of pathological events in Alzheimer's disease. Brain. 2009;132:1355–65.
17. Rinne JO, Brooks DJ, Rossor MN, Fox NC, Bullock R, Klunk WE, et al. 11C-PiB PET assessment of change in fibrillar amyloid-[beta] load in patients with Alzheimer's disease treated with bapineuzumab: a phase 2, double-blind, placebo-controlled, ascending-dose study. Lancet Neurol. 2010;9:363–72.
18. Shin J, Lee SY, Kim SH, Kim YB, Cho SJ. Multitracer PET imaging of amyloid plaques and neurofibrillary tangles in Alzheimer's disease. Neuroimage. 2008;43:236–44.
19. Agdeppa ED, Kepe V, Liu J, Flores-Torres S, Satyamurthy N, Petric A, et al. Binding characteristics of radiofluorinated 6-dialkylamino-2-naphthylethylidene derivatives as positron emission tomography imaging probes for beta-amyloid plaques in Alzheimer's disease. J Neurosci. 2001;21:RC189.
20. McKhann G, Drachman D, Folstein M, Katzman R, Price D, Stadlan EM. Clinical diagnosis of Alzheimer's disease: report of the NINCDS-ADRDA work group under the auspices of Department of Health and Human Services Task Force on Alzheimer's disease. Neurology. 1984;34:939–44.
21. Petersen RC, Smith GE, Waring SC, Ivnik RJ, Tangalos EG, Kokmen E. Mild cognitive impairment: clinical characterization and outcome. Arch Neurol. 1999;56:303–8.
22. Brix G, Zaers J, Adam LE, Bellemann ME, Ostertag H, Trojan H, et al. Performance evaluation of a whole-body PET scanner using the NEMA protocol. J Nucl Med. 1997;38:1614–23.
23. Wilson AA, Garcia A, Chestaskova A, Kung HF, Houle SA. A rapid one-step radiosynthesis of the beta-amyloid imaging radiotracer N-methyl-[C-11]2-(′4-methylaminophenyl)-6-hydroxybenzothiazole ([C-11]-6-OH-BTA-1). J Labelled Comp Radiopharm. 2004;47:679–82.
24. Klok RP, Klein PJ, van Berckel BNM, Tolboom N, Lammertsma AA, Windhorst AD. Synthesis of 2-(1,1-dicyanopropen-2-yl)-6-(2-[18F]-fluoroethyl)-methylamino-naphthalene ([18F]FDDNP). Appl Radiat Isot. 2008;66:203–7.
25. Svarer C, Madsen K, Hasselbalch SG, Pinborg LH, Haugbol S, Frokjaer VG, et al. MR-based automatic delineation of volumes of interest in human brain PET images using probability maps. Neuroimage. 2005;24:969–79.
26. Wu Y, Carson R. Noise reduction in the simplified reference tissue model for neuroreceptor functional imaging. J Cereb Blood Flow Metab. 2002;22:1440–52.
27. Yaqub M, Tolboom N, Boellaard R, van Berckel BNM, van Tilburg EW, Luurtsema G, et al. Simplified parametric methods for [11C]PIB studies. Neuroimage. 2008;42:76–86.
28. Yaqub M, Tolboom N, van Berckel BNM, Scheltens P, Lammertsma AA, Boellaard R. Simplified parametric methods for [18F]FDDNP studies. Neuroimage. 2010;49:433–41.
29. Yamaguchi H, Hirai S, Morimatsu M, Shoji M, Nakazato Y. Diffuse type of senile plaques in the cerebellum of Alzheimer-type dementia demonstrated by beta protein immunostain. Acta Neuropathol. 1989;77:314–9.
30. Jack Jr CR, Knopman DS, Jagust WJ, Shaw LM, Aisen PS, Weiner MW, et al. Hypothetical model of dynamic biomarkers of the Alzheimer's pathological cascade. Lancet Neurol. 2010;9:119–28.
31. Hardy JA, Selkoe DJ. The amyloid hypothesis of Alzheimer's disease: progress and problems on the road to therapeutics. Science. 2002;197:353–6.
32. Hyman BT, Marzloff K, Arriagada PV. The lack of accumulation of senile plaques or amyloid burden in Alzheimer's disease suggests a dynamic balance between amyloid deposition and resolution. J Neuropathol Exp Neurol. 1993;52:594–600.
33. Christie RH, Bacskai BJ, Zipfel WR, Williams RM, Kajdasz ST, Webb WW, et al. Growth arrest of individual senile plaques in a model of Alzheimer's disease observed by in vivo multiphoton microscopy. J Neurosci. 2001;21:858–64.
34. Bouwman FH, van der Flier WM, Schoonenboom NSM, van Elk EJ, Kok A, Rijmen F, et al. Longitudinal changes of CSF biomarkers in memory clinic patients. Neurology. 2007;69:1006–11.
35. Thompson PW, Ye L, Morgenstern JL, Sue L, Beach TG, Judd DJ, et al. Interaction of the amyloid imaging tracer FDDNP with hallmark Alzheimer's disease pathologies. J Neurochem. 2009;109:623–30.
36. Tolboom N, van der Flier WM, Yaqub M, Boellaard R, Verwey NA, Blankenstein MA, et al. Relationship of cerebrospinal fluid markers to 11C-PiB and 18F-FDDNP binding. J Nucl Med. 2009;50:1464–70.

37. Tolboom N, Flier WM, Yaqub M, Koene T, Boellaard R, Windhorst AD, et al. Differential association of [11C]PIB and [18F]FDDNP binding with cognitive impairment. Neurology. 2009;73:2079–85.
38. Alexander GE, Chen K, Pietrini P, Rapoport SI, Reiman EM. Longitudinal PET evaluation of cerebral metabolic decline in dementia: a potential outcome measure in Alzheimer's disease treatment studies. Am J Psychiatry. 2002;159:738–45.
39. Forster S, Grimmer T, Miederer I, Henriksen G, Yousefi BH, Graner P, et al. Regional expansion of hypometabolism in Alzheimer's disease follows amyloid deposition with temporal delay. Biol Psychiatry 2011. doi:10.1016/j.biopsych.2011.04.023
40. van der Vlies AE, Koedam ELGE, Pijnenburg YAL, Twisk JWR, Scheltens P, van der Flier WM. Most rapid cognitive decline in APOE E4 negative Alzheimer's disease with early onset. Psychol Med. 2009;39:1907–11.
41. Verhage F. Intelligentie en leeftijd: onderzoek bij Nederlanders van twaalf tot zevenenzeventig jaar [Intelligence and age: study with Dutch people aged 12 to 77]. Assen: Van Gorcum; 1964.